13th International Symposium on Particle Image Velocimetry – ISPIV 2019
Munich, Germany, July 22-24, 2019

Influence of Air-Jet Vortex Generators on Spatial Structures in a Shock Wave / Turbulent Boundary Layer Interaction

Deepak Prem Ramaswamy[1*] **and Anne-Marie Schreyer**[1]

[1] Institute of Aerodynamics, RWTH Aachen University, Aachen, Germany

[*] d.ramaswamy@aia.rwth-aachen.de

Abstract

We study the influence of an array of air-jet vortex generators on a 24^o compression-ramp interaction at Mach 2.5 and a free stream unit Reynolds number of $Re/m = 9.72 \times 10^6$. Focusing-schlieren and oil-flow visualisation were used to characterise the flow features, while particle image velocimetry was used to study the mean flow and turbulence of the interaction region. Further interpretation was carried out based on a snapshot proper orthogonal decomposition of the velocity fields for the baseline and the control cases, extracting the energetic coherent structures of the flow. The injection of the jets was found to redistribute the energy from the lower order modes to the higher order modes, while maintaining nearly similar structural distribution as the baseline case.

1 Introduction

Shock-wave boundary layer interactions are complex flow fields, pervasive in high speed aerospace applications like rocket engine nozzles, air-breathing engine inlets, external surfaces of supersonic and hypersonic vehicles etc. An adverse pressure gradient imposed by a strong shock wave can result in a large scale separation of the flow, thus resulting in high fluctuating pressure and thermal loads on the surface. This can directly affect the vehicle integrity, major design features and thus cost (Dolling, 2001). Therefore, many computational and experimental investigations were carried out in the past decade (Dolling, 2001; Delery and Marvin, 1986; Smits and Dussauge, 2006; Andreopoulos et al., 2000; Babinsky and Harvey, 2011; Clemens and Narayanaswamy, 2014) leading to significant improvements in understanding.

To reduce the adverse effects of shock-wave boundary layer interactions and to ensure safe vehicle operation, the research community has been actively involved in developing flow control approaches (Delery, 1985). One commonly studied approach is the employment of large or sub-boundary layer vanes or ramps, which act as vortex generators and induce streamwise vortices in the boundary layer (Pearcey, 1961). The streamwise vortices alter the boundary layer characteristics by redistributing the momentum within the boundary layer, making the boundary layer more resistant to separation. However, the physical presence of these objects in the flow may result in drag penalties. Moreover, these mechanical vortex generators are usually optimised only for particular flow conditions and cannot be 'switched off' when not needed. These disadvantages can be circumvented by incorporating air-jet vortex generators (AJVGs), first introduced by Wallis (1952). In this technique, steady jets of air are injected into the cross-stream, resulting in the formation of similar streamwise vortices in the flow (Kamotani and Greber, 1972). The AJVGs have been observed to show similar effectiveness as mechanical vane-type vortex generators (Wallis, 1952; Wallis and Stuart, 1958; Pearcey, 1961). A number of studies have attempted to characterise the influence of different parameters on the control effectiveness. Wallis (1952) and Wallis and Stuart (1958) showed that no streamwise component of injection is essential for effective control. Szwaba (2013) investigated various jet orifice diameters at transonic Mach numbers and concluded that an orifice diameter less than one fourth the boundary layer thickness resulted in significant reduction in separation length and shock amplitude. The investigations were later extended to the supersonic regime (Souverein and Debiève, 2010; Verma and Manisankar, 2012; Verma et al., 2014; Ramaswamy and Schreyer, 2019) exhibiting similarly promising behaviour.

Despite previous research efforts, the exact mechanism of AJVG control and the behavior of vortical structures due to jet injection is not completely understood yet. These interactions are characterised by various time and length scales. Studying the behaviour of the most energetic coherent structures will provide information on the governing mechanisms (Lumley, 1967; Berkooz et al., 1993) and thus pave the way for potent flow control. For this purpose, in the current study, snapshot proper orthogonal decomposition (Sirovich, 1987) is applied to velocity fields obtained from PIV to extract and analyse the most energetic coherent structures in the flow and to study the influence of AJVGs on these structures.

2 Experimental Setup

2.1 Flow facility:

Experiments were conducted in the trisonic wind tunnel facility at the Institute of Aerodynamics, RWTH Aachen University at a freestream Mach number of 2.5 and a freestream unit Reynolds number of $9.72 \times 10^6\ m^{-1}$. It is a suction type wind tunnel with a test section geometry of $0.4 \times 0.4\ m^2$. Air is evacuated from the vacuum tanks by a $400kW$ compressor and supplied to a settling balloon after passing through a silica gel drier. This ensures a relative humidity of well below 4%. By operating a fast-acting valve, a stable flow of about 3.5 seconds can be achieved for the configuration used in this study. The stagnation conditions of the flow are given by the ambient conditions in the laboratory and hence the selected Mach number determines the free-stream Reynolds number. Optical access is provided by circular windows on either side of the test section and on the top wall.

2.2 Wind tunnel model:

The wind tunnel model (Figure 1(a)) consists of a flat plate of $902mm$ length spanning the entire width of the test section, onto which a 24^o compression-ramp is installed. A zig-zag trip is placed at $10mm$ from the leading edge of the flat plate, to ensure a uniform turbulent boundary layer thickness of $\delta = 9.8mm$ at 4.59δ upstream of the ramp corner. The undisturbed boundary layer condition, along with the inflow conditions, are summarised in Table 1.

Table 1: Inflow and Boundary layer parameters

P_o	1 bar	δ	9.8mm
T_o	295 K	$\delta^*{}_c$	3.06mm
M_∞	2.5	θ_c	0.76mm
Re_∞	$9.72 \times 10^6 m^{-1}$	u_τ	26.3 m/s
U_∞	591 m/s	C_f	0.0019

An AJVG module with 23 circular orifices of $d_{jet} = 0.1\delta$ diameter is placed 8.16δ upstream of the ramp corner. The various parameters associated with the AJVGs are also depicted in Figure 1(a). For this investigation, the jets are pitched at an angle of $\phi = 45^o$ with respect to the flat-plate and skewed at an angle of $\theta = 90^o$ with respect to the freestream, thus resulting in a pure spanwise injection. This ensures comparability with the results from Wallis and Stuart (1958), Szwaba (2011, 2013, 2005) and Souverein and Debiève (2010). The 23 jet orifices of the AJVG module are equidistantly spaced with a spacing of $D = 0.82\delta$. A pressure plenum underneath the AJVG insert, supplies the air-jet array. The jets are injected with a pressure equal to the wind tunnel stagnation pressure with total mass flow rate of $\dot{m}_{AJVG} = 0.0041 kg/s$. This configuration showed the best control efficiency in our previous investigations (Ramaswamy et al., 2018).

2.3 Measurement techniques:

PIV measurements were carried out to generate a database for the POD analysis. Di-Ethyl-Hexyl-Sebacate (DEHS) particles are illuminated using a Quantel twins BSL Nd:YAG laser, with a maximum pulse energy of 140mJ. A field of view (FoV) of $8.16\delta \times 5.40\delta$ was covered with a PCO 4000 camera with a resolution of $4008px \times 2672px$, accommodating the entire separation region. The images were acquired with an acquisition frequency of $2.5Hz$. The pulse delay was chosen to be equal to $0.7\mu s$, resulting in a freestream particle displacement of about 20 pixels. Figure 1(b) shows the schematics of the PIV setup. In addition to PIV, oil-flow and focusing-schlieren visualisation were also used to study the global flow features. Further details of the measurement setup can be found in Ramaswamy and Schreyer (2019).

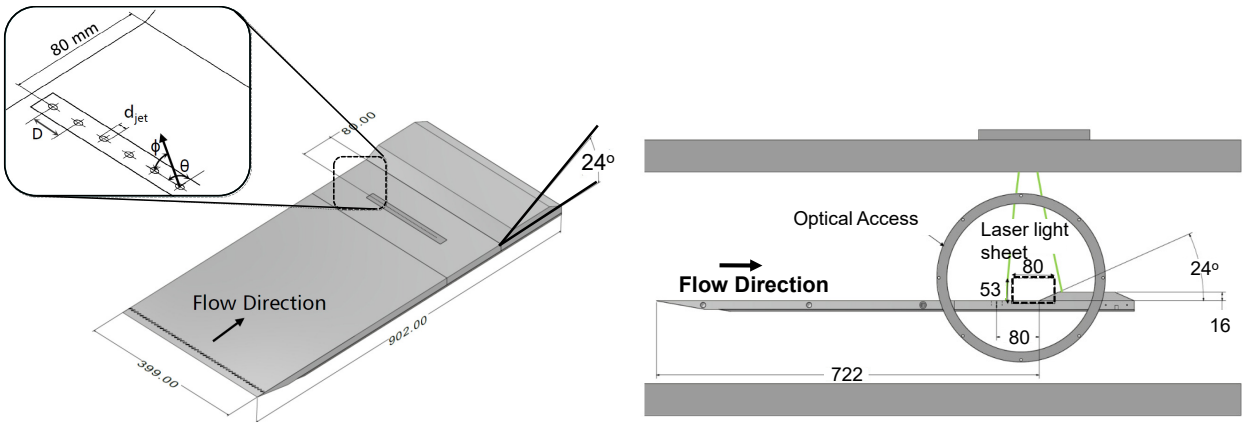

(a) Wind tunnel model.

(b) PIV setup. The dashed rectangle shows the camera FoV

Figure 1: Measurement set-up

3 Data Analysis

The raw particle images were first pre-processed by subtracting the minimum of each pixel from the series, which was then followed by dynamic histogram clipping. PIV analysis was carried out using the commercial software PIVView. A standard iterative multigrid algorithm was used to obtain the velocity vectors, with a final window size of $32px \times 32px$ at 75% overlap. A normalised median filter was used to detect spurious vectors, which were then replaced by the interpolation of the surrounding vectors.

The most energetic coherent structures characterize the behaviour of turbulent flows. These coherent structures can be extracted with proper orthogonal decomposition (POD) (Lumley, 1967; Berkooz et al., 1993). In this investigation, the snapshot POD technique introduced by Sirovich (1987) was applied to the velocity fields from PIV. Due to the low acquisition frequency, the instantaneous velocity fields are uncorrelated in time, and are thus suitable for this technique. The method of snapshots follows solving an eigenvalue problem relative to the averaged space cross-correlation tensor between two mean-subtracted velocity fields, thereby extracting spatial POD modes $\phi_n(\mathbf{x})$ and time-dependent orthonormal amplitude coefficients $a_n(t)$. The fluctuating components of velocity can then be reconstructed as follows:

$$\mathbf{u}(\mathbf{x},t) = \sum_{j=1}^{N} a_n(t)\phi_n(\mathbf{x}) \tag{1}$$

where N is the number of snapshots. Each mode is assigned a fraction of the contained energy and the obtained POD modes are sorted by descending energy content. Further details on the mathematical background of POD can be obtained from Berkooz et al. (1993).

4 Results and Discussion

4.1 Flow Topology

Fig. 2(a) shows a focusing-schlieren visualisation of the baseline case, depicting the typical features of a compression-ramp induced shock-wave/turbulent boundary layer interaction. The incoming boundary layer experiences an adverse pressure gradient due to the presence of the ramp and separates from the surface with the formation of a separation shock. The separated shear layer then reattaches on the ramp surface and encloses a large recirculation region. The surface features of the baseline case can also be seen in the oil flow visualisation in Fig. 2(b) where the separation and the reattachment lines are clearly visible. The flow is observed to separate 4.12δ upstream of the ramp corner and reattaches 1.44δ downstream of the corner, resulting in a total separation length of 5.56δ, measured along the local surface directions.

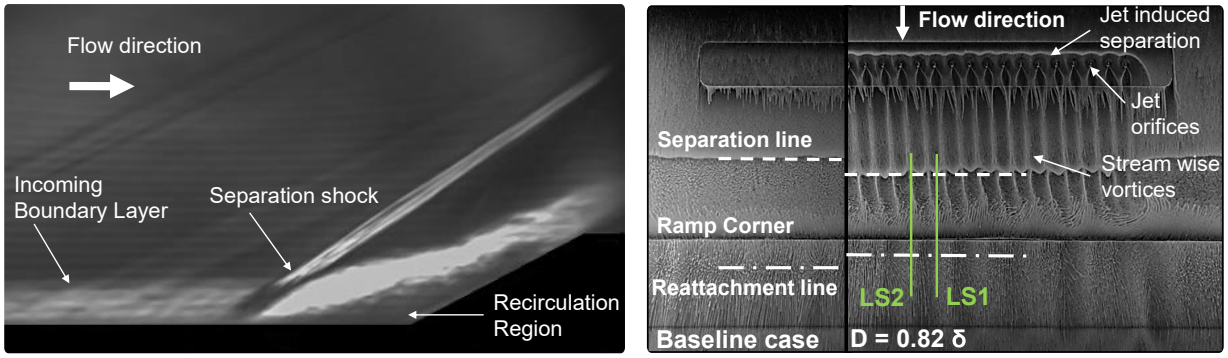

(a) Focusing schlieren visualisation of the baseline case depicting the global flow features

(b) Effect of AJVG control on the separation region. Green lines indicate the spanwise location of laser light sheet

Figure 2: Flow topology of the interaction region with and without control. Image taken and modified from Ramaswamy and Schreyer (2019)

The oil-flow visualisation in Fig. 2(b) (right) also shows the effect of AJVGs with $D = 0.82\delta$ on the interaction region. At the injection location, the jets impose an obstruction to the incoming flow which leads to local separation. The injection of the jets into the cross-flow results in the formation of streamwise vortices and leads to the formation of high and low speed streaks close to the wall as seen by the streaky oil-pattern. This leads to a corrugated separation line, with regions of lower and higher local separation lengths. A parametric study has been conducted (Ramaswamy et al., 2018) to investigate the influence of jet spacing on the control efficiency. AJVGs of jet spacings varying from $D = 0.41\delta$ to $D = 2.56\delta$ were studied. At a jet spacing of $D = 0.82\delta$, the effectiveness was the best with a downstream movement of the separation line with respect to the uncontrolled case by 7.8%. For these further investigations, PIV was carried out on this most effective configuration.

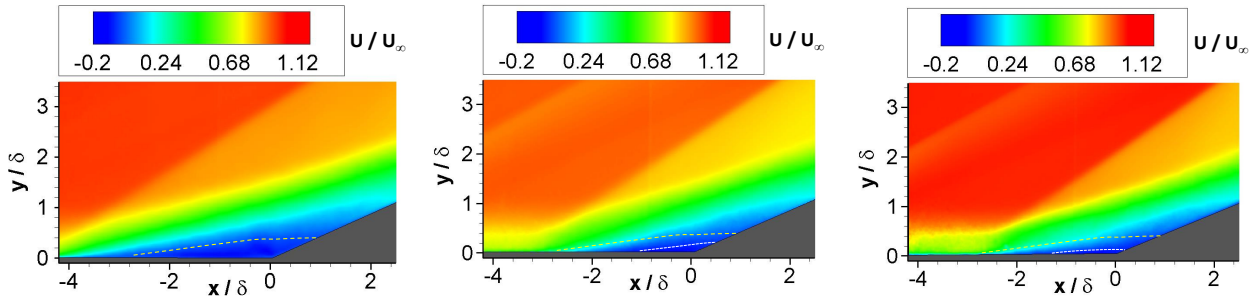

(a) Baseline Case

(b) Control case - LS1

(c) Control case - LS2

Figure 3: Contours of the normalised mean streamwise velocity component. Yellow dashed lines depict the contour of zero velocity for the baseline case while the white dotted lines depict the same for the corresponding control cases. Image adapted from Ramaswamy and Schreyer (2019)

Due to the strong three dimentionality of the flow, the control case was investigated at two spanwise locations (see Fig. 2(b)). Position LS1 lies along the centreline of the jet orifice at the centreline of the model ($z = 0$) and position LS2 lies in between two jet orifices ($z = -1.22\delta$). Fig 3 shows contours of the mean streamwise velocity components in the streamwise direction for both the uncontrolled and the control cases. A massive separation bubble can be observed for the baseline case, which is substantially reduced under the influence of control. Turbulence measurements taken at several streamwise locations both upstream and downstream of the ramp corner (not shown here) indicate a marginal reduction of turbulence intensity maxima under the influence of control, especially after flow reattachment. For a detailed discussion on the mean flow and turbulence of the interaction region, the reader is referred to Ramaswamy and Schreyer (2019).

4.2 POD Analysis

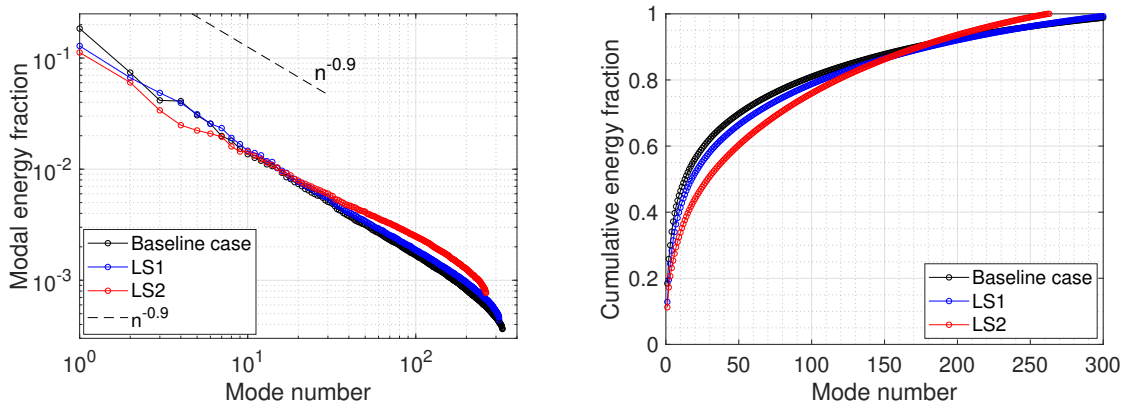

(a) Energy fraction of each mode

(b) Cumulative modal energy

Figure 4: Eigenvalue spectrum of snapshot POD analysis with and without AJVG control

In order to extract the coherent structures, the previously discussed snapshot POD technique was applied to the obtained PIV data for both the baseline case and the LS1 and LS2 cases. The resulting eigenvalue spectrum and the cumulative energy fraction for n number of modes is shown in Fig. 4. The eigenspectra show a clear and typical decrease of energy, with the first few modes contributing to the majority of the energy. The first mode alone accounts for nearly 10% to 20% of the total energy for each case. For the baseline case, the first 13 modes account for nearly 50% of the total energy. This number tends to be higher under the influence of control, with the first 18 and 29 modes accounting for about 50% of the total energy for LS1 and LS2 respectively. The eigenspectra also show that with the application of AJVG control, a reduction of modal energy fraction with respect to the baseline case is observed for the lower order modes while an increase in energy is observed for the higher order modes. The POD eigenspectra show a rapid decrease of energy proportional to $n^{-0.9}$, which is consistent with the observations of Piponniau et al. (2012).

The POD modes of the normalised streamwise and wall normal fluctuating velocity components for a series of lower and higher order modes are shown in Figs. 5–8, respectively. The intermediate POD modes which exhibit similar spacial organisation are not shown. For all reported cases, energetic structures are observed only in the boundary layer, along the shock and in the separated shear layer. For the baseline case, the most energetic first mode of the streamwise component represents the velocity fluctuations in the separation shear layer and the recirculation bubble. Modes 2 - 4 show large regions of alternating velocity fluctuations, close to the separated region, the reattachment region and in the separation bubble (see Figs. 5(d),(g),(j)). The spacial organisation of these dominant modes agree well with previous reports in literature (Mustafa et al., 2019). A significant portion of the turbulent kinetic energy is also observed in the location of the separation shock (see Figs. 5(j) and 6(d)) due to its low-frequency oscillation, which is a typical feature of this interaction (Clemens and Narayanaswamy, 2014). This is also evident in the POD modes of the wall normal velocity fluctuations in Figs. 7 and 8 where the large energy content in the shock wave is clearly visible. At higher order modes, e.g. mode 25 (Fig 6(j)), several small alternating regions of velocity fluctuations are visible in the separation region of the baseline case, depicting the small scale coherent structures in the flow, with increasingly smaller structures observed with increase in mode numbers.

Figs. 5–8 also show the POD modes of the streamwise and wall-normal velocity components of the control case, at both LS1 (centre column) and LS2 (right column) positions. No pronounced variation in the spacial organisation of the POD modes are evident compared with the uncontrolled baseline case. The most energetic mode 1 for the control case (Figs. 5(b) and 5(c)) also represents the separated shear layer, similar to the baseline case. However, a smaller streamwise extent, especially upstream of the ramp corner is observed (Figs. 5(b) and 5(c)). This is due to the downstream movement of the separation line under the influence of control. Consequently, a small portion of the boundary layer upstream of the separation shock becomes visible with a structure similar to the uncontrolled case. Modes 2-4 (Figs. 5(e),(f),(h),(i),(k),(l)) in the control case also represent alternating regions of velocity fluctuations with a structure similar to the uncontrolled

case. A small but significant portion of energy for the control case is associated with the jet-induced shock, which is clearly depicted in the POD modes of the wall-normal velocity components (Figs. 7(e) and 7(h)).

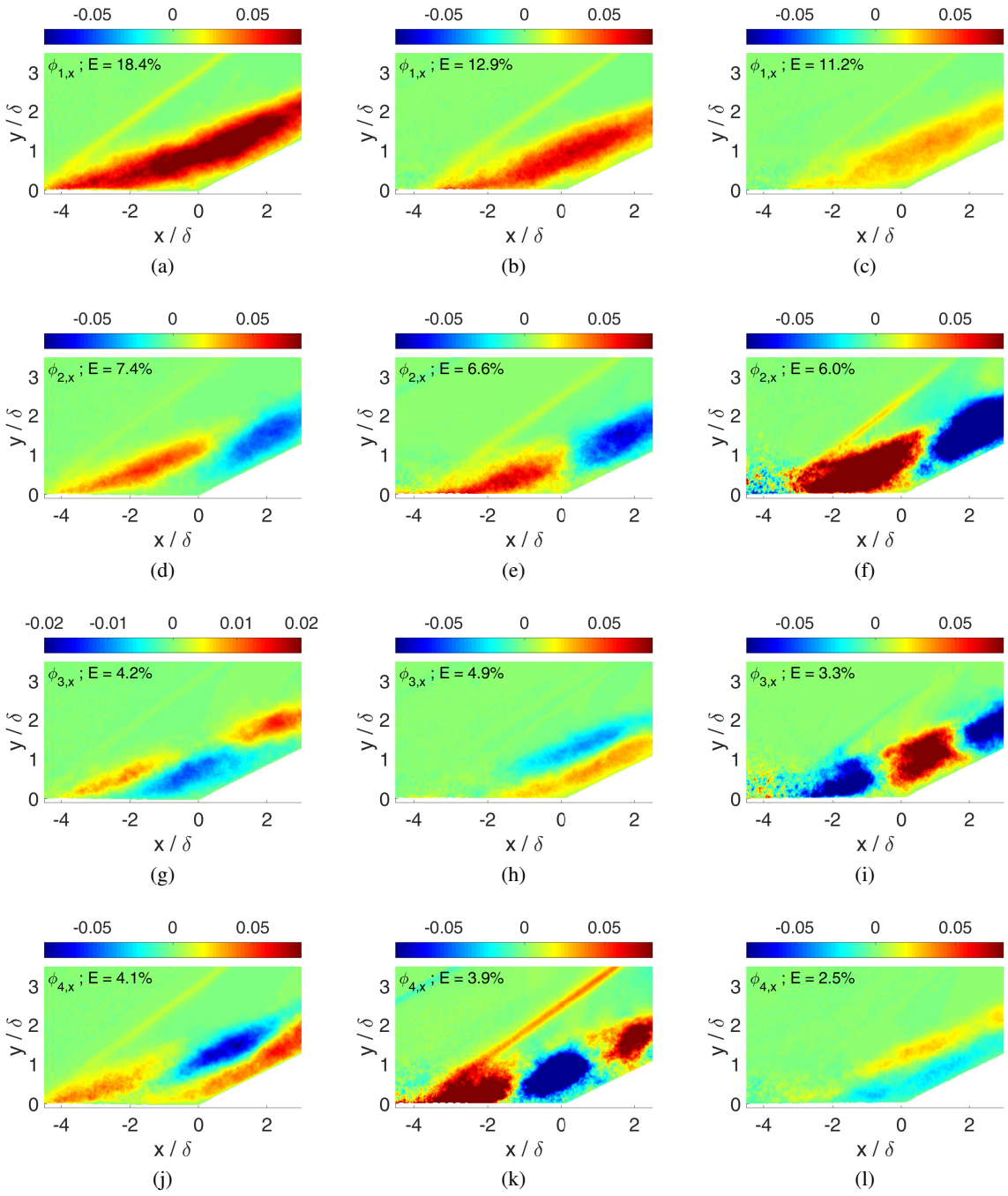

Figure 5: POD modes (1 - 4) of $\frac{u'}{U_\infty}$ for the baseline case (left), LS1 (middle) and LS2 (right)

The observations based on the POD analysis suggest that the injection of the jets tends to decrease the modal energy fraction of the lower order modes, which is then shifted to higher-order modes. This suggests a transfer of energy from the separation and reattachment zones to the turbulent structures shed downstream. This has previously been observed by Schreyer et al. (2017). However, this energy redistribution does not have any impact on the overall spacial organisation of the structures, with both the baseline and the control

cases portraying very similar coherent structure distributions.

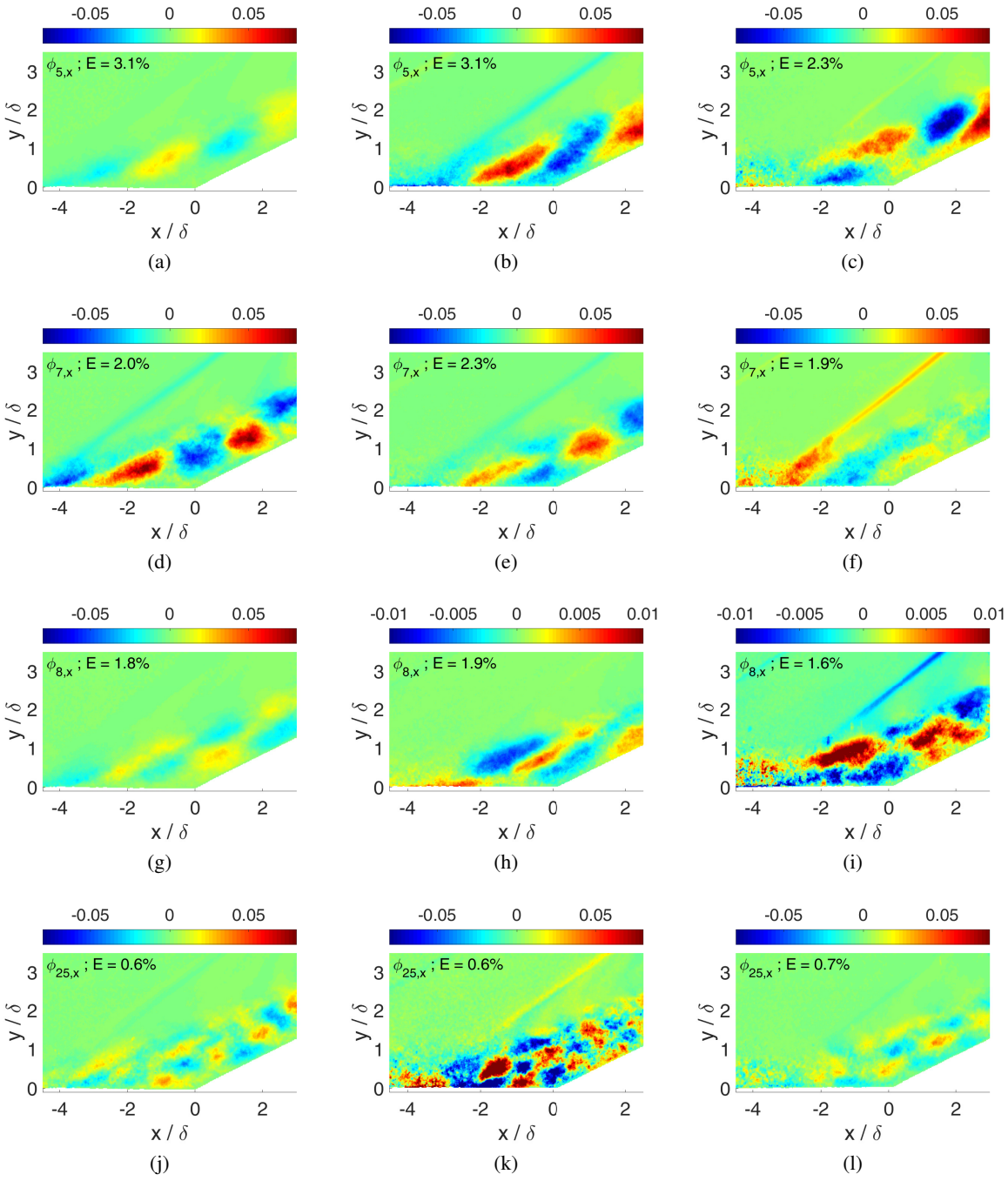

Figure 6: POD modes (5 - 25) of $\frac{u'}{U_\infty}$ for the baseline case (left), LS1 (middle) and LS2 (right)

5 Conclusion

We studied the influence of an array of air-jet vortex generators on a shock-wave/turbulent boundary layer interaction at a 24^o compression ramp at $M_\infty = 2.5$ and $Re/m = 9.72 \times 10^6$. Particular focus was given to

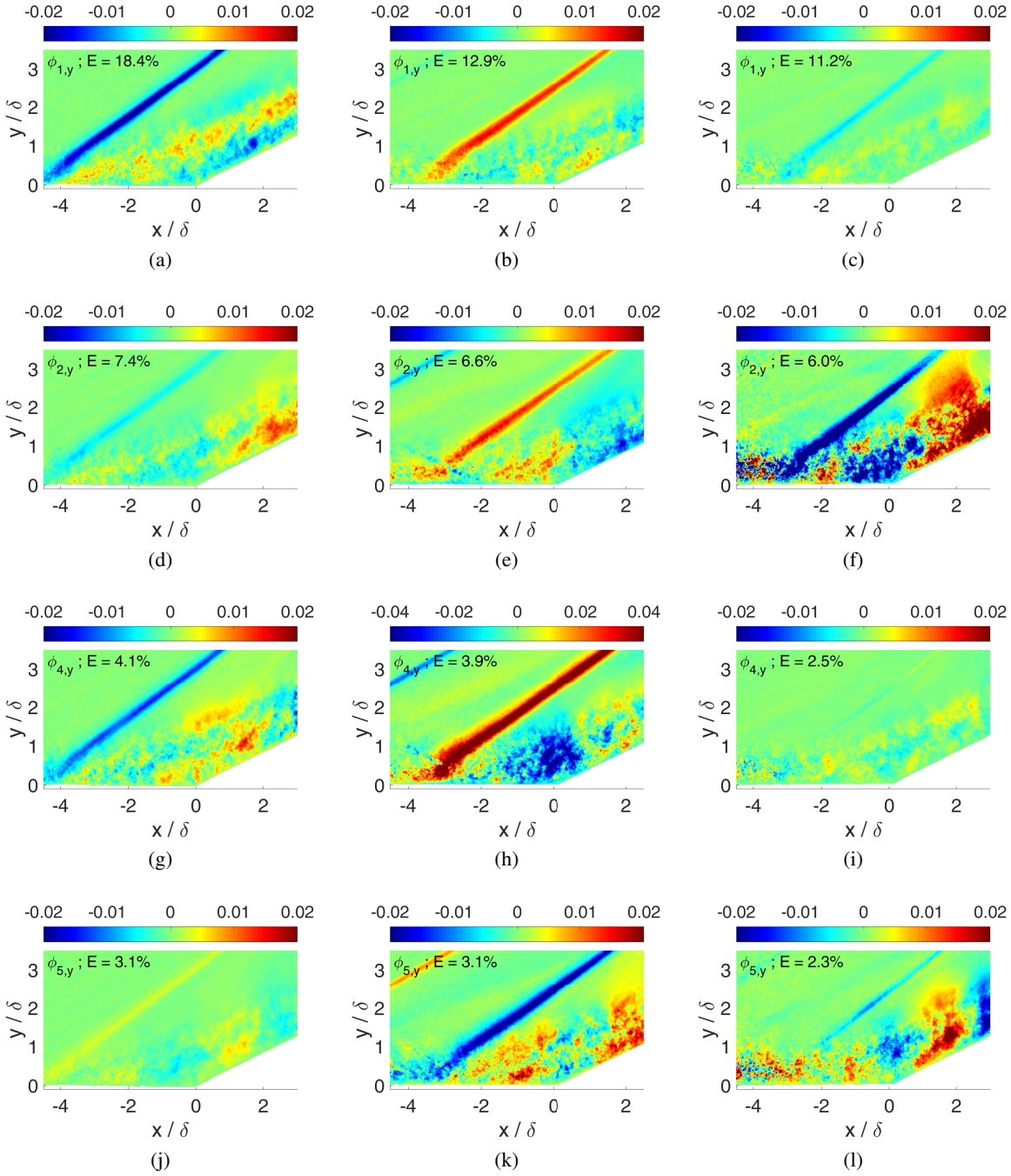

Figure 7: POD modes (1 - 5) of $\frac{v'}{U_\infty}$ for the baseline case (left), LS1 (middle) and LS2 (right)

the behaviour and development of coherent structures with and without jet injection. The snapshot proper orthogonal decomposition technique was applied to the velocity fields obtained from PIV, thus extracting the most energetic structures of the flow. The first few modes representing the shear layer, separation and reattachment regions contain the bulk of the energy. Under the influence of control, there is a shift of modal energy from the lower order modes to the higher order modes representing the turbulent structures in the boundary layer shed downstream, while leaving the spatial organisation of the coherent structures largely unaffected and similar to the corresponding modes of the baseline case.

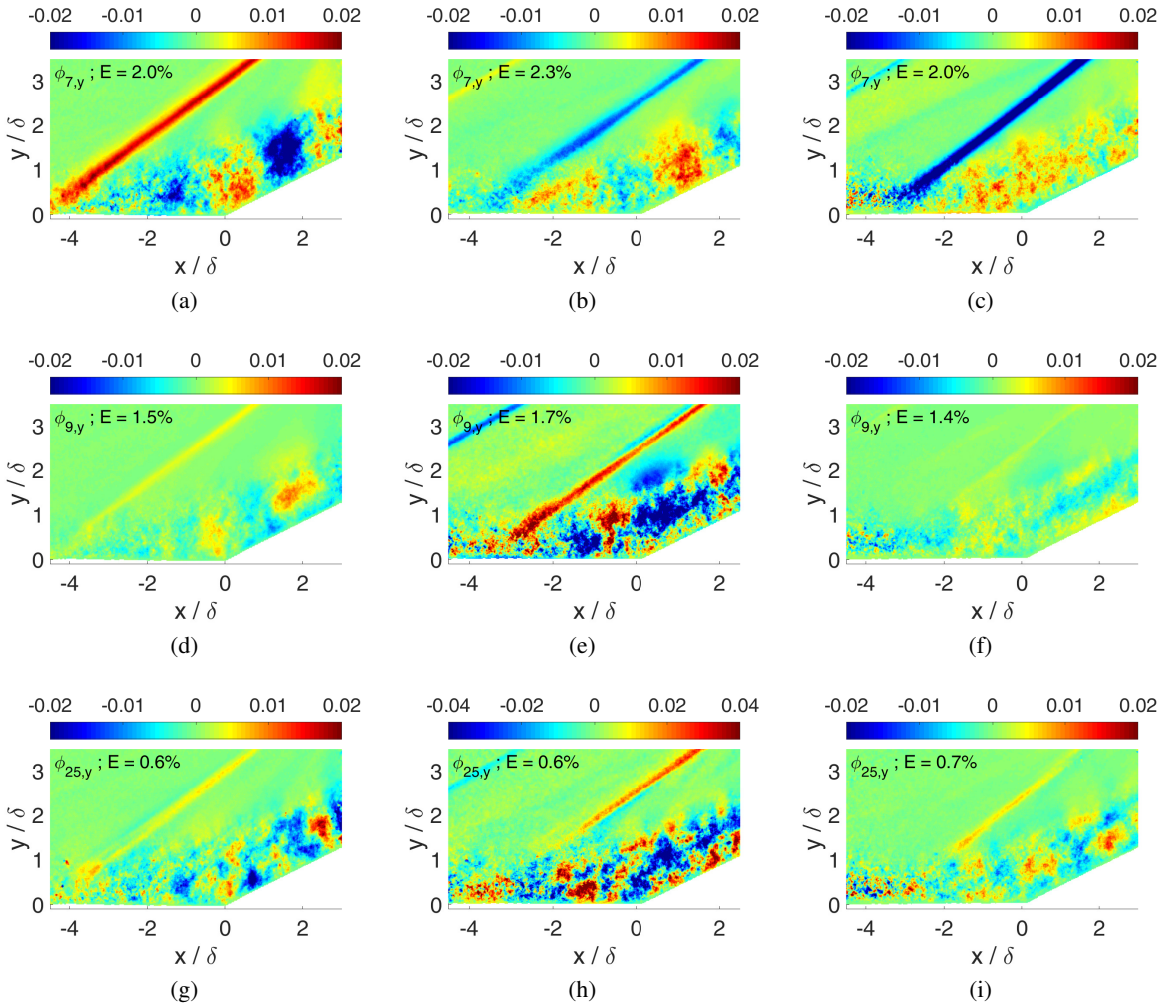

Figure 8: POD modes (7 - 25) of $\frac{v'}{U_\infty}$ (left) for the baseline case (left), LS1 (middle) and LS2 (right)

Acknowledgements

This work was funded by the German Research Foundation (DFG) in the framework of the Emmy Noether Programme (grant SCHR 1566/1-1). The contribution to the experimental setup by Nick Capellmann and the workshop is greatly appreciated.

References

Andreopoulos Y, Agui JH, and Briassulis G (2000) Shock Wave—Turbulence Interactions. *Annual Review of Fluid Mechanics* 32:309–345

Babinsky H and Harvey J, editors (2011) *Shock wave-boundary-layer interactions*. Cambridge aerospace series. Cambridge University Press, Cambridge

Berkooz G, Holmes P, and Lumley JL (1993) The Proper Orthogonal Decomposition in the Analysis of Turbulent Flows. *Annual Review of Fluid Mechanics* 25:539–575

Clemens NT and Narayanaswamy V (2014) Low-frequency unsteadiness of shock wave/turbulent boundary layer interactions. *Annual Review of Fluid Mechanics* 46:469–492

Delery J and Marvin JG (1986) Shock-wave boundary layer interactions. *AGARDograph* AGARD-AG-280

Delery JM (1985) Shock wave/turbulent boundary layer interaction and its control. *Progress in Aerospace Sciences* 22:209–280

Dolling DS (2001) Fifty Years of Shock-Wave/Boundary-Layer Interaction Research: What Next?. *AIAA Journal* 39:1517–1531

Kamotani Y and Greber I (1972) Experiments on a Turbulent Jet in a Cross Flow. *AIAA Journal* 10:1425–1429

Lumley JL (1967) The Structure of Inhomogeneous Turbulence. in AM Yaglom and VI Tatarski, editors, *Atmospheric Turbulence and Wave Propagation*. pages 166–178

Mustafa MA, Parziale NJ, Smith MS, and Marineau EC (2019) Amplification and structure of streamwise-velocity fluctuations in compression-corner shock-wave/turbulent boundary-layer interactions. *Journal of Fluid Mechanics* 863:1091–1122

Pearcey HH (1961) Shock Induced Separation and its Prevention by Design and Boundary Layer control. in GV Lachmann, editor, *Boundary Layer and Flow Control*. volume II. pages 1170–1355. Pergamon Press

Piponniau S, Collin E, Dupont P, and Debiève JF (2012) Reconstruction of velocity fields from wall pressure measurements in a shock wave/turbulent boundary layer interaction. *International Journal of Heat and Fluid Flow* 35:176–186

Ramaswamy DP, Hinke R, and Schreyer AM (2018) Influence of jet spacing and injection pressure on separation control with air-jet vortex generators. in *21st DGLR-FAch Symposium of the STAB, Darmstadt*

Ramaswamy DP and Schreyer AM (2019) Effect of Jet Spacing in Separation Control with Air Jet Vortex Generators. in *AIAA Scitech 2019 Forum, 7-11 January 2019, San Diego, California.*

Schreyer AM, Dussauge JP, and Krämer E (2017) Characterization of an incipiently separated shock wave/turbulent boundary layer interaction. *Shock Waves* 27:153–168

Sirovich L (1987) Turbulence and the dynamics of coherent structures. Part I-III. *Quarterly of Applied Mathematics* 45:561–590

Smits AJ and Dussauge JP (2006) *Turbulent Shear Layers in Supersonic Flow*. Springer-Verlag, New York. 2nd edition

Souverein LJ and Debiève JF (2010) Effect of air jet vortex generators on a shock wave boundary layer interaction. *Experiments in Fluids* 49:1053–1064

Szwaba R (2005) Shock wave induced separation control by streamwise vortices. *Journal of Thermal Science* 14:249–253

Szwaba R (2011) Comparison of the influence of different air-jet vortex generators on the separation region. *Aerospace Science and Technology* 15:45–52

Szwaba R (2013) Influence of air-jet vortex generator diameter on separation region. *Journal of Thermal Science* 22:294–303

Verma SB and Manisankar C (2012) Shockwave/Boundary-Layer Interaction Control on a Compression Ramp Using Steady Micro Jets. *AIAA Journal* 50:2753–2764

Verma SB, Manisankar C, and Akshara P (2014) Control of shock-wave boundary layer interaction using steady micro-jets. *Shock Waves* 25:535–543

Wallis RA (1952) The use of air jets for boundary layer control. Aero Note 110. Aeronautical Research laboratories

Wallis RA and Stuart CM (1958) On the Control of Shock-Induced Boundary Layer Separation with Discrete Air Jets. Aeronautical Research Council CP 595